Dielectric Barrier Discharges revisited: the case for mobile surface charge

F. J. J. Peeters[1], R. F. Rumphorst[2], M. C. M. van de Sanden[1,2]

[1]FOM institute DIFFER, P.O. Box 1207, 3430 BE, Nieuwegein, The Netherlands
[2]Eindhoven University of Technology, Department of Applied Physics, POB 513, NL-5600 MB Eindhoven, The Netherlands
(e-mail: f.j.j.peeters@differ.nl)

Abstract

We propose a mechanism to explain many features of the multi-filament dielectric barrier discharge: while part of the charge deposited during previous discharge cycles is immobile on the dielectric over time periods of seconds, the larger fraction of the deposited charge must be mobile on time-scales of hundreds of ns. For alumina, we estimate that a sheet resistance of 3 MΩ/sq is consistent with the multi-filament discharge; an increase in conductivity of at least 12 orders of magnitude. The existence of this type of plasma-induced surface conductivity could prove relevant in modeling a wide range of plasma devices, in addition to DBD.

Dielectric Barrier Discharges (DBDs) in filamentary mode consist of many small, transient microdischarges with diameters of ~ 0.1 mm and durations on the order of 20 - 100 ns, distributed over the dielectric [1]. Each filament leads to current pulses with peak plasma currents up to 100 mA, giving rise to extreme current densities of up to several 100 A/cm^2 to the dielectric surface. In this letter, the link between the discrete current pulses of individual filaments and the seemingly continuous behavior of the discharge averaged over many filaments in both space and time is discussed. Note that DBD can also operate in a homogeneous glow, or glow-like mode, depending on gas mixture or the characteristics of the driving voltage [2–4]. Our analysis of the charging behavior of the dielectric given here is focused on the filamentary mode, though the results should be equally applicable to the glow modes. Under sinusoidal driving voltage, measurements of the charge in the filamentary DBD, Q, with respect to the external voltage, V, lead to parallelogram-shaped Q-V diagrams with a well-defined slope ζ_{diel} during the discharge period, see Figure 1. The slope ζ_{diel} is lower than, or equivalent to, the dielectric capacitance C_{diel}, because the discharge may cover less than the available dielectric area in each half-cycle [5]. In 1943, Manley showed that the Q-V parallelogram could be modeled by assuming a constant gap voltage during discharge half-cycles [6]. Peeters *et al.* have further shown that this gap voltage, termed the burning voltage U_b, does not change significantly as a function of applied voltage amplitude [5], suggesting that filaments occurring at different phases of the applied voltage are electrically equivalent. In [7] it was shown that because of this constant U_b, the only control over N_2 dissociation in DBD is achieved by changing the density of filaments, while the characteristics of the filaments are set by the geometry of the system. While the dynamics of individual filaments have been studied in detail, both through experiment and modeling [1,8–10], the multi-filament discharge is rarely treated. From the point of view of *individual* filaments, the plasma current is naturally limited by the rate at which charges can be conductively transferred from the dielectric surface to the opposing electrode. The transfer of charge across the gap also negates the electric field sustaining the discharge, thus always reducing the current to zero over time. However, even in the absence of pre-existing charge on the dielectric, there is no *a priori* reason why multiple filaments could not form simultaneously across the surface, provided they are sufficiently separated. This could lead to very high total (peak) currents through the DBD system, over a time period of a few nanoseconds. Manley's electrical model does not consider that the dielectric surfaces in DBDs can donate or deposit charge and that the plasma current is only limited by the rate of change of this deposited charge Q_d:

$$i_{plasma}(t) = \frac{\partial Q_d(t)}{\partial t}. \qquad (2)$$

In other words, if there is a *local* current $i_{plasma}(t)$ flowing through the gap, the *local* charge state $Q_d(t)$ of the insulating dielectric surface is changing at a corresponding rate. Current through the dielectric is therefore always consistent with the plasma current, and there is essentially no maximum to the plasma current dictated by the external voltage. Manley's circuit provides a model for multi-filament discharges, but not an explanation for the mechanism behind these discharges. Of course, in a practical system the plasma current would be limited by the current that can be supplied by the power source, but for a well-designed system this is never the limiting factor for the plasma current. Why then does discharging of the dielectric occur in such a way that individual current pulses lead to an average slope ζ_{diel} in Q-V diagrams, as depicted schematically in Figure 1 and observed experimentally in all cases involving sinusoidal driving voltage [6]? Furthermore, the existence of a constant burning voltage U_b throughout a discharge half-cycle implies that individual filaments ignite at approximately the same critical voltage, irrespective of the external voltage at each point in time. This constant burning voltage

throughout the discharge half-cycle is commonly attributed to the surface charge deposited on the dielectric by individual filaments. These surface charges persist between discharge cycles and affect the next series of filamentary discharges when the applied voltage is reversed [11]. Self-organization of the surface charge is the preferred explanation of this phenomenon, but rigorous calculations showing that this can lead to constant burning voltages are lacking. Gibalov *et al.* model a surface-DBD for multiple filaments with pre-existing surface charges, with good agreement to measurements, but the relationship between surface charge and current pulses and the reproducibility from cycle to cycle is not discussed [12]. Chirokov *et al.* model multi-filament interaction with a quasi-empirical Monte-Carlo simulation with good qualitative agreement with the experimentally obtained spatial distributions of the filaments, but electrical characteristics are not presented [13]. Xu and Kushner present a model to calculate the dynamics of up to 4 overlapping filaments at the surface [14]. The evolution of the charge state of the surface over many cycles is not modeled, however, and only the interaction between near-simultaneous filaments is studied. The evolution of the surface charge for a DBD in He over 24 discharge cycles is calculated by Stollenwerk *et al*, with excellent qualitative correspondence to experimental Lichtenberg images [15]. However, these results are applicable to self-organized patterns in glow-like discharges, where the plasma filaments form simultaneously in each discharge cycle, a phenomenon clearly distinct from the filamentary discharges which are the subject here [3].

Using a DBD setup with an area of 7 mm^2, small enough to contain no more than ~ 30 filaments per half-cycle, we can distinguish individual filaments in *Q-V* diagrams. The DBD, depicted in Figure 2, employs a custom generator and transformer circuit, providing sinusoidal applied voltages with peak-to-peak amplitudes between 1 - 10 kV_{pp} at a frequency of 100 kHz to a brass top (primary) electrode of 3.0 mm diameter, which is adjustable in height to provide various gap widths. The bottom (secondary) electrode also has a diameter of 3.0 mm and is covered by dielectric material, which here consists of alumina of 1.0 or 0.6 mm thickness and a relative permittivity, $\varepsilon_r = 9.8 \pm 0.2$. The surface area of the dielectric material is large with respect to the electrode area so that it always extends beyond the edges of the electrodes. To prevent unwanted discharging underneath the dielectric, the space around the secondary electrode is insulated using a Teflon ring, with silicone gel providing an air-tight seal. The DBD is operated in ambient air, with no humidity control. We measure three signals, the applied voltage $V(t)$ and two voltages, $V_1(t)$ and $V_2(t)$, in an electrical circuit between DBD and ground. The difference $V_1(t) - V_2(t)$ is the voltage drop across a measurement capacitor $C_{meas} = 4.3$ nF, and is used to determine the charge $Q(t)$ in the system via:

$$Q(t) = C_{meas} \cdot (V_1(t) - V_2(t)) \tag{3}$$

The voltage $V_2(t)$ over a 400 Ω, 750 pF RC-circuit is fed into a Pulse Height Analyzer (PHA) circuit used to count the number of filaments per half-cycle of the applied voltage and to obtain statistical distributions of the transferred charge per filament in the DBD [16].

Figure 3 shows representative *Q-V* diagrams and charge/filament distributions for the small DBD. In Figure 3(a) individual steps making up the slope ζ_{diel} can be clearly distinguished in the positive half-cycle, while the negative half-cycle shows evidence of an Atmospheric Pressure Townsend Discharge (APTD) [17]. The APTD emerges because during the negative half-cycle the metal electrode is the cathode, leading to more uniform emission of electrons compared to when the dielectric is the cathode. Figure 3(b) shows that for the positive half-cycle, there is no significant difference between charge/filament distributions as a function of applied voltage amplitude and only the number of filaments increases. Previous studies have found similar results, but usually single filament distributions are measured in pin-to-pin geometries [18,19], or very low filament number densities are measured in square centimeter-sized DBDs at low applied voltages [20–24]. Figure 3(b) implies that individual filaments remain roughly equivalent, independent of the external voltage, the number of filaments, or the pre-existing deposited charge density.

By applying the equivalent circuit of [5] to the overall slopes ζ_{diel} of the stepped *Q-V* diagrams as depicted in Figure 3(a), the average surface coverage β of the discharge can be determined, as well as the fractional area covered by a single filament [5]. In Figure 4 we plot the surface coverage β as a function of filament density $N/A_{discharge}$, simultaneously determined using the PHA circuit, and find similar behavior for all the DBD configurations studied. Note that the maximum discharge area is an effective value, determined by taking the slope $\zeta_{diel} = C_{diel}$ at $\beta = 1$, which implies the entire electrode area is discharged, and assuming the ideal plane-parallel capacitor formula:

$$A_{\text{discharge}} = C_{diel} d_{diel} / \varepsilon_0 \varepsilon_r. \tag{4}$$

The maximum effective discharge area is slightly different for each DBD geometry, with $A_{\text{discharge}}$ between 9 and 12 mm^2. While this is a crude approximation, the goal is to provide only a qualitative picture of the development

of multi-filament discharges. Depicted in Figure 4 is a power law fit of the data, serving as a guide to the eye, along with two simulations. Both simulations are based on individual filament footprints covering a constant fractional area $a_{filament}/A_{discharge}$. The fractional area for a single filament is determined from Figure 4 to be between 0.15 and 0.20, depending on the DBD configuration. The first simulation is the maximum coverage that can be attained by N overlapping circles, while the second simulation gives the average coverage attained by N circles if their placement within the discharge area is entirely random, averaged over 1000 cycles. Both simulations are illustrated in Figure 5 for $N = 8$ and $a_{filament}/A_{discharge} = 0.17$. What we conclude from comparing these simulations to the data is that filaments do not occur randomly across the surface, but tend to spread out as much as possible. Nevertheless, there is always a significant overlap between filament footprints, starting at $N > 2$. In our experiments we have up to 30 filaments occurring within a half-cycle, suggesting each part of the dielectric surface is (dis-)charged up to 5 times, or 30 x 0.17, without significantly affecting the transferred charge per filament or the burning voltage for each consecutive filament.

The behavior of the multi-filament discharge as described in this paper is consistent with the development of the surface charge as depicted in Figure 6, which is discussed step-by-step below. The discussion is aimed specifically at cathode-directed streamers, for which (net) negative charge is extracted from the dielectric.

(1) A filament will preferentially form at locations of increased charge density. Filament ignition will occur when the gap voltage equals the burning voltage U_b, which, with increasing external voltage, will occur first at the point of highest net negative charge density at the surface. These peak charges, referred to as 'memory charges' and indicated in green in Figure 6, are static on time-scales of seconds, or remaining immobile for at least longer than one cycle. Most of the net charge at the surface can be considered laterally mobile, however, on time-scales of 100's of ns and is referred to as 'mobile charge', indicated in red in Figure 6. The possible physical origins of the memory and mobile charges are discussed at the end of this letter. If there is a significant contribution of APTD to the negative half-cycle, the initial memory charge peak in this step may be absent, because APTD is expected to charge the dielectric surface uniformly.
(2) As the filament interacts with the surface and the surface expansion occurs, negative charge is locally extracted from the surface, which reduces the burning voltage U_b across the surface expansion region. Both the mobile negative charge and the memory charge are locally reduced, and the latter can become (partially) inverted, accounting for the memory effect during the next half-cycle.
(3) Between steps (1) and (3) only several tens of nanoseconds have passed. This time scale is too short for the mobile charge to have redistributed significantly, due to its limited mobility. Redistribution of this charge mostly occurs after the filament is decaying. If charges would have a too high mobility, the filament would not extinguish because the local gap voltage (burning voltage U_b) can be maintained until all mobile charge on the dielectric surface is removed, or until the external voltage begins to decrease.
(4) After a time > 100 ns, the mobile charges will again be distributed uniformly on the surface. The gap voltage will have been reduced over an area >> $a_{filament}$. The external voltage has to be increased by an amount dV before the next filament can ignite at the critical gap voltage U_b.

The charge distribution before and after discharging in steps (1) and (4) in Figure 6 is consistent with the charge patterns measured directly by Bogaczyk *et al.* using a BSO crystal as dielectric in a He/N_2 DBD [25–27]. Their measurements show mostly flat charge distributions interspersed by Gaussian peaks at the locations of the filaments, where both the uniform charge and the Gaussian peaks become inverted after each half-cycle is completed. Using a steady-state model, Heinisch *et al.* show that for a dielectric with positive electron affinity, such as alumina with $\chi = 2.5$ eV, electrons populate the conduction band and can, therefore, result in mobile charge [28,29]. Mobility of deposited surface charge has been experimentally observed by Wild *et al.* over several centimeters and is argued to take place within or on the surface of the material and not via the gas-phase [30]. We calculate that a sheet resistance R_S of 3 MΩ/sq is required to allow for a description of the multi-filament discharge with the equivalent circuit of Figure 1(b); an increase in conductivity of at least 12 orders of magnitude compared to bulk alumina [16]. Assuming electrons are the majority carrier, the required 2D electron density n_e^{2D} to achieve this low sheet resistance can be calculated via:

$$n_e^{2D} = (eR_S\mu_e)^{-1}, \tag{5}$$

with e the electron charge and μ_e the electron mobility. With μ_e in 400K alumina on the order of 10^{-5} to 10^{-3} m^2/Vs [31,32], we can estimate that $n_e^{2D} = 10^{17}$ - 10^{15} m^{-2}. Given that a filament deposits ~1 nC of charge over an area $a_{filament} \approx 10^{-6}$ m^2, or ~10^{16} m^{-2}, the expected level of conductivity can be achieved. Mobile electrons in the conduction band can quickly become trapped in localized impurities or intrinsic trap states at energies 0.5 – 0.9

eV below the conduction band and give rise to non-uniform 'memory charges' centered at the locations of filaments [31,33,34]. Similarly, positive charging can occur via e.g. recombination with positive ions and capture by $N_2(A\ ^3\Sigma_u^+)$ metastables [28,35,36]. With a density of trap states of 10^{24} m^{-3} [31,37], a penetration depth of charge carriers of 1 nm would lead to 10^{15} m^{-2} of memory charge, less than or equal to the expected mobile charge density. While we have no direct measurement of memory charge in this work, it is a necessary feature of any model in order to account for memory effect and the stochastic component of filamentary DBDs, *e.g.* differences in charge/pulse between filaments. As stated by Heinisch and Bronold *et al.* in [28], the time-scales on which charges are trapped in a dielectric are directly related to the states in which they are trapped, with both questions requiring further theoretical and experimental study. Whether the redistribution of surface charges described here has an effect on the glow or glow-like modes remains to be verified, though it can be expected that redistribution reduces inhomogeneity of the surface charge distribution and thereby suppresses the transition to the filamentary discharge mode, see e.g. [2].

To summarize, the behavior of multi-filament DBD cannot be accounted for with the assumption of purely static surface charges, as is commonly assumed in models, but requires the existence of mobile surface charges. Considering the relatively extreme plasma conditions occurring at the dielectric surface, specifically the high current densities associated with filamentary discharges, makes the filamentary DBD an interesting model system for studying the interaction of plasma with dielectric surfaces. Since many plasma devices and plasma processing techniques involve dielectric surfaces to some degree, further fundamental study of charge-carrier related plasma-surface interaction may prove relevant for a large number of applications.

[1] Kogelschatz U 2003 Dielectric-barrier Discharges : Their History , Discharge Physics , and Industrial Applications *Plasma Chem. Plasma Process.* **23** 1–46

[2] Golubovskii Y B, Maiorov V A and Behnke J F 2003 On the stability of a homogeneous barrier discharge in nitrogen relative to radial perturbations *J. Phys. D. Appl. Phys.* **36** 975–81

[3] Stollenwerk L, Amiranashvili S, Boeuf J-P and Purwins H-G 2007 Formation and stabilisation of single current filaments in planar dielectric barrier discharge *Eur. Phys. J. D* **44** 133–9

[4] Somekawa T, Shirafuji T, Sakai O, Tachibana K and Matsunaga K 2005 Effects of self-erasing discharges on the uniformity of the dielectric barrier discharge *J. Phys. D. Appl. Phys.* **38** 1910–7

[5] Peeters F J J and van de Sanden M C M 2015 The influence of partial surface discharging on the electrical characterization of DBDs *Plasma Sources Sci. Technol.* **24** 015016

[6] Manley T C 1943 The electric characteristics of the ozonator discharge *Trans. Electrochem. Soc.* **84** 83–96

[7] Peeters F J J, Yang R and van de Sanden M C M 2015 The relation between the production efficiency of nitrogen atoms and the electrical characteristics of a dielectric barrier discharge *Plasma Sources Sci. Technol.* **24** 045006

[8] Bruggeman P and Brandenburg R 2013 Atmospheric pressure discharge filaments and microplasmas: physics, chemistry and diagnostics *J. Phys. D. Appl. Phys.* **46** 464001

[9] Wagner H-E, Brandenburg R, Kozlov K V, Sonnenfeld A, Michel P and Behnke J F 2003 The barrier discharge: basic properties and applications to surface treatment *Vacuum* **71** 417–36

[10] Wagner H-E, Yurgelenas Y V. and Brandenburg R 2005 The development of microdischarges of barrier discharges in N 2 /O 2 mixtures—experimental investigations and modelling *Plasma Phys. Control. Fusion* **47** B641–54

[11] Kogelschatz U 2010 Collective phenomena in volume and surface barrier discharges *J. Phys. Conf. Ser.* **257** 012015

[12] Gibalov V I and Pietsch G J 2004 Properties of dielectric barrier discharges in extended coplanar electrode systems *J. Phys. D. Appl. Phys.* **37** 2093–100

[13] Chirokov A, Gutsol A, Fridman A, Sieber K D, Grace J M and Robinson K S 2004 Analysis of two-dimensional microdischarge distribution in dielectric-barrier discharges *Plasma Sources Sci. Technol.* **13** 623–35

[14] Xu X P and Kushner M J 1998 Multiple microdischarge dynamics in dielectric barrier discharges *J. Appl. Phys.* **84** 4153

[15] Stollenwerk L, Amiranashvili S, Boeuf J-P and Purwins H-G 2006 Measurement and 3D Simulation of Self-Organized Filaments in a Barrier Discharge *Phys. Rev. Lett.* **96** 255001

[16] Peeters F J J 2015 *The electrical dynamics of dielectric barrier discharges* (Eindhoven University of Technology)

[17] Naudé N, Cambronne J-P, Gherardi N and Massines F 2005 Electrical model and analysis of the transition from an atmospheric pressure Townsend discharge to a filamentary discharge *J. Phys. D. Appl. Phys.* **38** 530–8

[18] Höft H, Kettlitz M, Hoder T, Weltmann K-D and Brandenburg R 2013 The influence of O2 content on the spatio-temporal development of pulsed driven dielectric barrier discharges in O2/N2 gas mixtures *J. Phys. D. Appl. Phys.* **46** 095202
[19] Akishev Y, Aponin G, Balakirev A, Grushin M, Karalnik V, Petryakov A and Trushkin N 2011 Role of the volume and surface breakdown in a formation of microdischarges in a steady-state DBD *Eur. Phys. J. D* **61** 421–9
[20] Jidenko N, Petit M and Borra J P 2006 Electrical characterization of microdischarges produced by dielectric barrier discharge in dry air at atmospheric pressure *J. Phys. D. Appl. Phys.* **39** 281–93
[21] Gibalov V I, Dřímal J, Wronski M and Samoylovich V G 1991 Barrier Discharge The Transferred Charge and Ozone Synthesis *Contrib. to Plasma Phys.* **31** 89–99
[22] Gibalov V I and Pietsch G J 2012 Dynamics of dielectric barrier discharges in different arrangements *Plasma Sources Sci. Technol.* **21** 024010
[23] Dřímal J, Gibalov V I and Samoylovich V G 1987 The magnitude of the transferred charge in the silent discharge in oxygen *Czechoslov. J. Phys. B.* **37** 1248–55
[24] Dřímal J 1988 On value of transferred charge in silent discharge under atmospheric pressure *Czechoslov. J. Phys. B.* **38** 159–65
[25] Bogaczyk M, Wild R, Stollenwerk L and Wagner H-E 2012 Surface charge accumulation and discharge development in diffuse and filamentary barrier discharges operating in He, N 2 and mixtures *J. Phys. D. Appl. Phys.* **45** 465202
[26] Bogaczyk M, Nemschokmichal S, Wild R, Stollenwerk L, Brandenburg R, Meichsner J and Wagner H-E 2012 Development of Barrier Discharges: Operation Modes and Structure Formation *Contrib. to Plasma Phys.* **52** 847–55
[27] Brandenburg R, Bogaczyk M, Höft H, Nemschokmichal S, Tschiersch R, Kettlitz M, Stollenwerk L, Hoder T, Wild R, Weltmann K-D, Meichsner J and Wagner H-E 2013 Novel insights into the development of barrier discharges by advanced volume and surface diagnostics *J. Phys. D. Appl. Phys.* **46** 464015
[28] Bronold F X, Fehske H, Heinisch R L and Marbach J 2012 Wall Charge and Potential from a Microscopic Point of View *Contrib. to Plasma Phys.* **52** 856–63
[29] Heinisch R L, Bronold F X and Fehske H 2012 Electron surface layer at the interface of a plasma and a dielectric wall *Phys. Rev. B* **85** 075323
[30] Wild R, Benduhn J and Stollenwerk L 2014 Surface charge transport and decay in dielectric barrier discharges *J. Phys. D. Appl. Phys.* **47** 435204
[31] Pickard P S and Davis M V. 1970 Analysis of Electron Trapping in Alumina Using Thermally Stimulated Electrical Currents *J. Appl. Phys.* **41** 2636
[32] Semenyuk L N 1996 Electrical properties of alumina films *Inorg. Mater.* **32** 1310–1
[33] Ambrico P F, Ambrico M, Colaianni a, Schiavulli L, Dilecce G and De Benedictis S 2010 Thermoluminescence study of the trapped charge at an alumina surface electrode in different dielectric barrier discharge regimes *J. Phys. D. Appl. Phys.* **43** 325201
[34] Ambrico P F, Ambrico M, Schiavulli L, Ligonzo T and Augelli V 2009 Charge trapping induced by plasma in alumina electrode surface investigated by thermoluminescence and optically stimulated luminescence *Appl. Phys. Lett.* **94** 051501
[35] Marbach J, Bronold F X and Fehske H 2012 Resonant charge transfer at dielectric surfaces *Eur. Phys. J. D* **66** 106
[36] Marbach J, Bronold F X and Fehske H 2012 Pseudoparticle approach for charge-transferring molecule-surface collisions *Phys. Rev. B* **86** 115417
[37] Novikov Y N, Gritsenko V A and Nasyrov K A 2009 Charge transport mechanism in amorphous alumina *Appl. Phys. Lett.* **94** 3–5

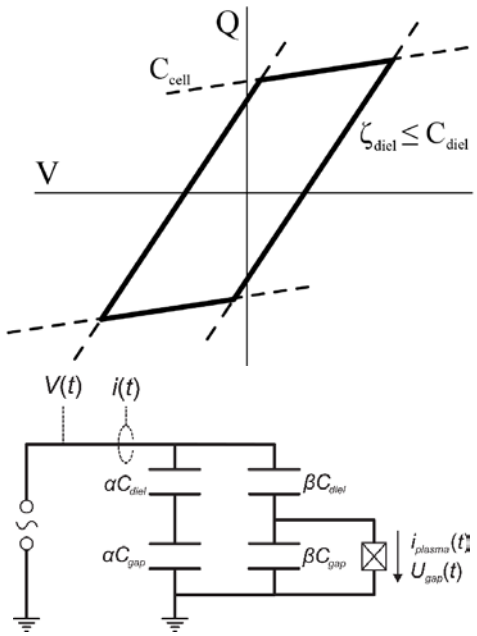

Figure 1: (a) Schematic Q-V diagram of a DBD under sinusoidal driving voltage. (b) Equivalent circuit of a DBD for variable surface coverage β of filaments. For $\beta = 1$ and $\alpha = \beta - 1 = 0$, Manley's original circuit is obtained.

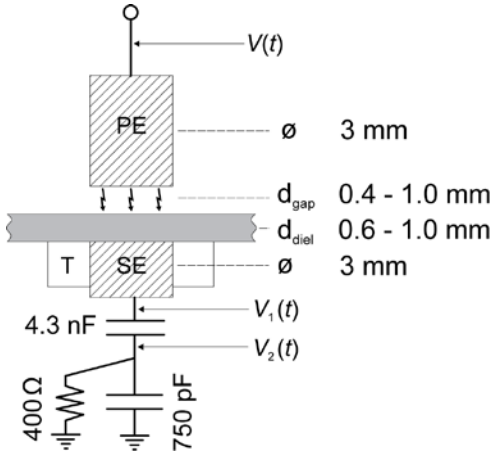

Figure 2: Schematic of the DBD setup, with the primary electrode, secondary electrode and Teflon ring indicated as PE, SE and T, respectively.

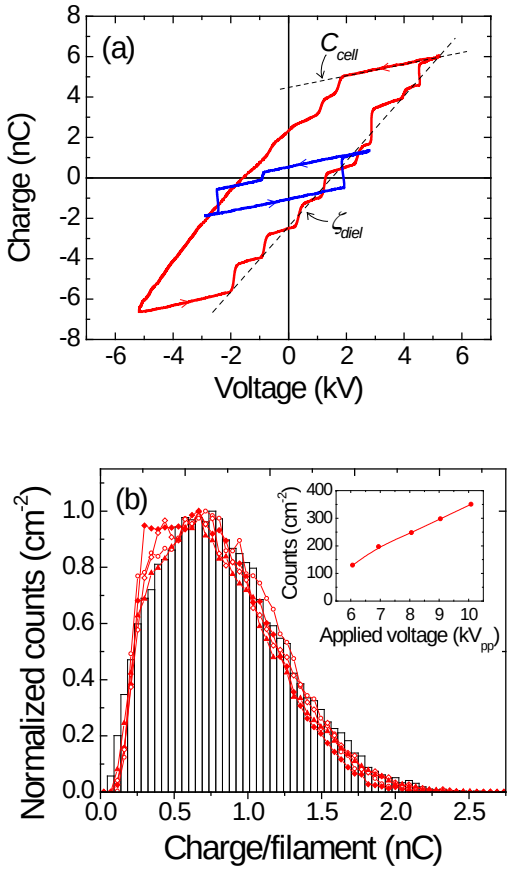

Figure 3: (a) Single-shot Q-V diagrams of an asymmetric DBD with 0.6 mm alumina and a 0.6 mm gap width at applied voltage amplitudes of 6 kV_{pp} (blue) and 10 kV_{pp} (red). Individual filamentary discharges are clearly distinguishable in the positive half-cycle. (b) Normalized charge per filament distributions with 0.6 mm alumina and a 0.4 mm gap width during the positive half-cycle for amplitudes of 6, 7, 8, 9 and 10 kV_{pp}. The inset shows the increasing filament number density with applied voltage.

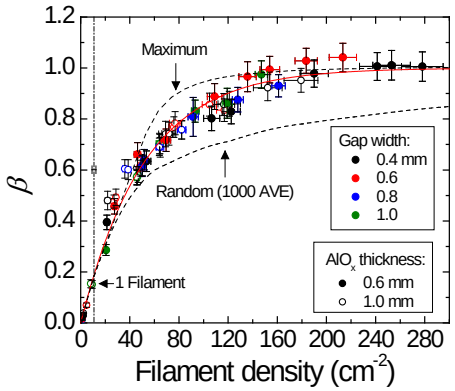

Figure 4: Average surface coverage of the discharge β as a function of filament density $N/A_{discharge}$ during the positive half-cycle. The red line is a guide to the eye, while the two dashed lines are models.

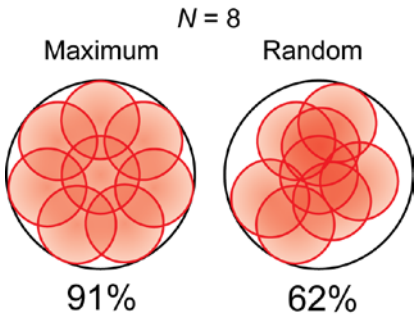

Figure 5: Illustration of maximum and random surface coverage attained by overlapping circles.

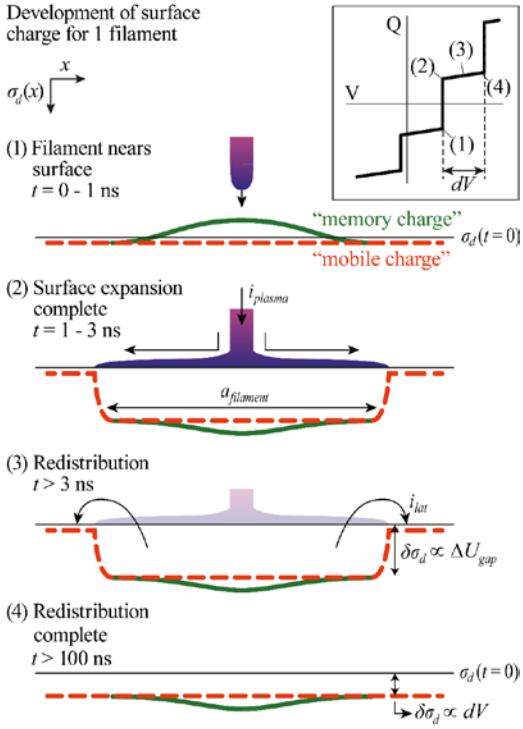

Figure 6: Schematic development of the net surface charge density σ_d for a single filament. The inset shows a segment of a Q-V diagram with the approximate occurrences of steps (1)-(4).